Inorg. Chem. **2008**, *47*, 4015−4022

P123-Assisted Hydrothermal Synthesis and Characterization of Rectangular Parallelepiped and Hexagonal Prism Single-Crystalline MgO with Three-Dimensional Wormholelike Mesopores

Guozhi Wang,[†] Lei Zhang,[†] Hongxing Dai,*[,†] Jiguang Deng,[†] Caixin Liu,[†] Hong He,[†] and Chak Tong Au*[,‡]

Laboratory of Catalysis Chemistry and Nanoscience, Department of Chemistry and Chemical Engineering, Beijing University of Technology, Beijing 100022, China, and Department of Chemistry, Hong Kong Baptist University, Kowloon Tong, Hong Kong, China

Received August 3, 2007

By adopting the strategy of dissolution−recrystallization under hydrothermal conditions (at 240 °C for 72 h) in the presence of a triblock copolymer (Pluronic P123), we fabricated nano- and microparticles of single-crystalline MgO of rectangular parallelepiped and hexagonal prism morphologies. The MgO crystallites display three-dimensional wormholelike mesopores and have a surface area as high as 298 m^2/g even after calcination at 550 °C for 3 h.

1. Introduction

In recent years, the fabrication and structures of various MgO materials have become a focus of research activities. The driving force is the high demand of MgO materials that are of large specific surface area. Due to the unique basic properties of MgO, the materials have been used in the fields of catalysis and toxic waste remediation.[1] There are cases in which bulk magnesium oxide was used as a catalyst for interesting and meaningful reactions.[2] In order to obtain MgO of large specific surface area, researchers used a number of methods for the fabrication of porous MgO materials.[3] According to a CMK-3 carbon-based exotemplating approach, Roggenbuck and Tiemann synthesized a mesoporous MgO material that is thermally highly stable.[3e] The pores of the MgO material are ordered and uniform and the distribution of pore size narrow. Nevertheless, the morphology and porosity of the as-prepared material depend heavily on the nature of the adopted template (i.e., SBA-15 and CMK-3), and the strategy for synthesis is rather complicated and the yield of the mesoporous material low. Another approach of generating mesoporous MgO is via a dissolution−recrystallization procedure with bulk MgO powders as the starting material.[3g] In the process, the MgO → $Mg(OH)_2$ reaction occurs under hydrothermal conditions, and the $Mg(OH)_2$ → MgO reaction takes place during calcination. Despite the fact that the route is simple and wormholelike mesoporous MgO can be produced on a large scale, the as-obtained material is rather low in surface area (around 100 m^2/g).[3g] It is known that disordered mesoporous materials with channels interconnected in a three-dimensional (3D) wormholelike fashion have advantages over their ordered counterparts. The former show better diffusion of reactants and products and are better than the latter in terms of mass-transfer limitation.[4a] In view of the enhanced accessibility of the reactant molecules to the active centers, the 3D wormholelike mesoporous materials (e.g., those of the MSU-X family) are believed to be superior to their ordered hexagonal analogues (e.g., SBA-15 and MCM-41) in catalytic performance.[4b] With the goal of generating the desired 3D wormholelike mesoporous MgO materials, we developed a surfactant-templated hydrothermal dissolution−recrystallization method. Herein, we report the fabrication and characterization of the rectangular parallelepiped and hexagonal

* Authors to whom correspondence should be addressed. E-mail address: hxdai@bjut.edu.cn (H.X.D.); pctau@hkbu.edu.hk (C.T.A.).
† Beijing University of Technology.
‡ Hong Kong Baptist University.

(1) (a) Rajagopalan, S.; Koper, O.; Decker, S.; Klabunde, K. J. *Chem.−Eur. J.* **2002**, *8*, 2602. (b) Choudary, B. M.; Mulukutla, R. S.; Klabunde, K. J. *J. Am. Chem. Soc.* **2003**, *125*, 2020. (c) Diwald, O.; Knözinger, E. *J. Phys. Chem. B* **2002**, *106*, 3495. (d) Anpo, M.; Yamada, Y.; Kubokawa, Y.; Coluccia, S.; Zecchina, A.; Che, M. *J. Chem. Soc., Faraday Trans.* **1988**, *84*, 751. (e) Murphy, D. M.; Farley, R. D.; Purnell, I. J.; Rowlands, C. C.; Yacob, A. R.; Paganini, M. C.; Giamello, E. *J. Phys. Chem. B* **1999**, *103*, 1944.
(2) (a) Zhang, G.; Hattori, H.; Tanabe, K. *Appl. Catal., A* **1988**, *36*, 189. (b) Di Cosimi, J. I.; Diez, V. K.; Apestegula, C. R. *Appl. Catal., A* **1996**, *137*, 149.

10.1021/ic7015462 CCC: $40.75
Published on Web 04/22/2008

prism MgO single crystallites with 3D wormholelike mesoporous architectures.

2. Experimental Section

Synthesis. The porous single-crystalline MgO samples were synthesized according to the method of surfactant-assisted hydrothermal interaction using ordinary MgO powders as the starting material. In a typical synthesis, 3.45 g of the poly(ethylene glycol)−poly(propylene glycol)−poly(ethylene glycol) triblock copolymer (Pluronic P123; Aldrich) was dissolved in 60 mL of deionized water; then, 0.8 g of MgO powders (Beijing Duli Chem., 99.5%) was added. The molar ratio of MgO to P123 adopted was 1:1.25. After being ultrasonically stirred for 24 h, the solution was transferred to a 50-mL Teflon-lined stainless steel autoclave of 40 mL packed volume for hydrothermal treatment at a selected temperature (160, 200, or 240 °C) for 24 or 72 h. The solid substance was filtered out and washed three to four times with deionized water and ethanol (for the removal of the majority of the surfactant) and then dried in an oven at 80 °C overnight. The as-obtained material was the $Mg(OH)_2$ precursor. After being ground thoroughly, the $Mg(OH)_2$ sample was heated in the air from room temperature to 550 °C at a rate of 1 °C/min and kept at 550 °C for 3 h for the generation of the MgO sample.

Characterization. Powder X-ray diffraction (XRD) patterns of the as-received MgO and $Mg(OH)_2$ samples were recorded on a Bruker/AXS D8 Advance X-ray diffractometer operated at 40 kV and 200 mA using Cu Kα radiation and a Ni filter. Diffraction peaks were referred to the powder diffraction files−1998 ICDD PDF Database−for phase identification. Surface areas and pore size distributions as well as N_2 adsorption−desorption isotherms of the samples were measured via N_2 adsorption at −196 °C on a Micromeritics ASAP 2020 apparatus with the samples outgassed at 250 °C for 2 h under a vacuum prior to measurement; surface areas and pore size distributions were calculated according to the Brunauer−Emmett−Teller (BET) and Barrett−Joyner−Halenda methods, respectively. The investigation by means of high-resolution scanning electron microscopy (HRSEM) was conducted on JEOL JSM 6500F and Gemini Zeiss Supra 55 equipment operated at 10 kV. The high-resolution transmission electron microscopy (HRTEM) images and selected area electron diffraction (SAED) patterns of the samples were collected on a JEOL-2010 instrument (operated at 200 kV). The thermogravimetric analysis (TGA) and differential scanning calorimetric (DSC) analysis were conducted in a flow of N_2 at a ramp of 10 °C/min on a SDT Q600 instrument (TA).

3. Results and Discussion

3.1. Structure and Morphology. Figure 1 shows the XRD pattern and HRSEM micrograph of the raw MgO powders. One can see that there was a small amount of $Mg(OH)_2$ impurity (Figure 1A), plausibly due to the hydration of MgO in the ambient environment. The raw MgO particles exhibit an irregular morphology with a size ranging from 50 to 100 nm (Figure 1B). Shown in Figure 2 are the wide-angle XRD patterns of the as-synthesized MgO and $Mg(OH)_2$ samples. The diffraction signals can be indexed to cubic MgO and hexagonal $Mg(OH)_2$ crystallites, and the lattice parameters are in good agreement with the standard values of JCPDS files (Nos. 45-946 and 7-239). The XRD signals of the MgO samples (Figure 2a−e) derived hydrothermally at 160, 200, or 240 °C with and without the use of P123 and calcined at 550 °C for 3 h show similar XRD patterns. Nonetheless,

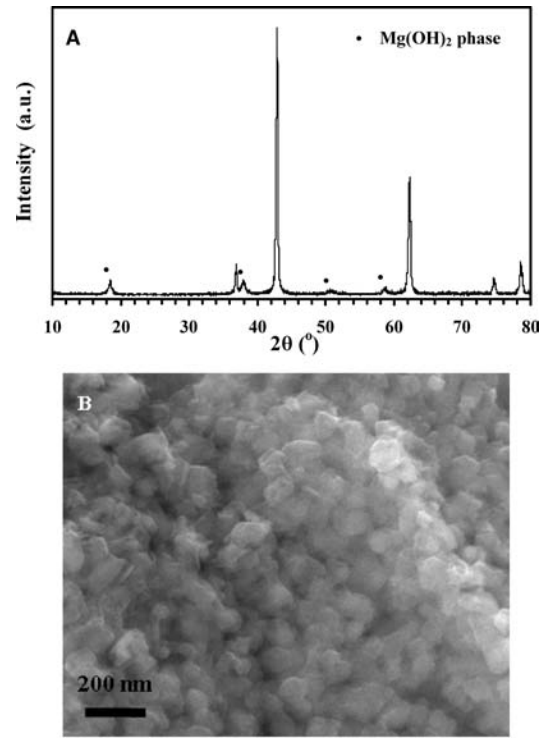

Figure 1. (A) XRD pattern and (B) HRSEM image of the raw MgO powders employed in the present study.

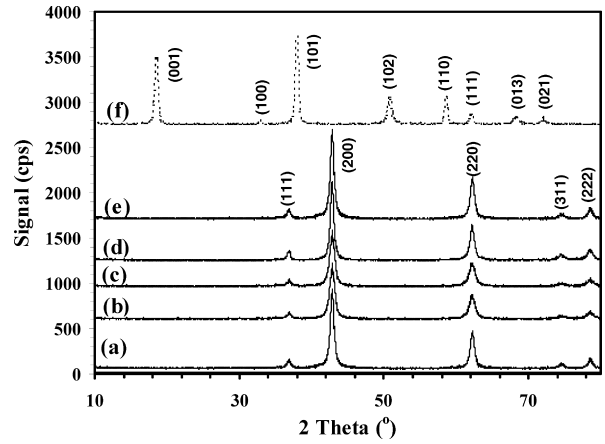

Figure 2. XRD patterns of MgO samples generated hydrothermally and calcined at 550 °C for 3 h (a) without P123 at 160 °C for 24 h, (b) with P123 at 160 °C for 72 h, (c) with P123 at 200 °C for 72 h, (d) without P123 at 240 °C for 72 h, and (e) with P123 at 240 °C for 72 h and (f) that of $Mg(OH)_2$ collected after hydrothermal treatment with P123 at 240 °C for 72 h without calcination.

(3) (a) Henrist, C.; Mathieu, J. P.; Vogels, C.; Rulmont, A.; Cloots, R. *J. Cryst. Growth* **2003**, *249*, 321. (b) Van Aken, P. A.; Langenhorst, F. *Eur. J. Mineral.* **2001**, *13*, 329. (c) Ding, Y.; Zhang, G. T.; Wu, H.; Hai, B.; Wang, L. B.; Qian, Y. T. *Chem. Mater.* **2001**, *13*, 435. (d) Utamapanya, S.; Klabunde, K. J.; Schlup, J. R. *Chem. Mater.* **1991**, *3*, 175. (e) Roggenbuck, J.; Tiemann, M. *J. Am. Chem. Soc.* **2005**, *127*, 1096. (f) Richards, R.; Li, W. F.; Decker, S.; Davidson, C.; Koper, O.; Zaikovski, V.; Volodin, A.; Rieker, T.; Klabunde, K. J. *J. Am. Chem. Soc.* **2000**, *122*, 4921. (g) Yu, J. C.; Xu, A.; Zhang, L.; Song, R.; Wu, L. *J. Phys. Chem. B* **2004**, *108*, 64.

(4) (a) Sinha, A. K.; Seelan, S.; Tsubota, S.; Haruta, M. *Angew. Chem., Int. Ed.* **2004**, *43*, 1546. (b) Zhai, S.; Zheng, J.; Shi, X.; Zhang, Y.; Dai, L.; Shan, Y.; He, M.; Wu, D.; Sun, Y. *Catal. Today* **2004**, *93*−*95*, 675.

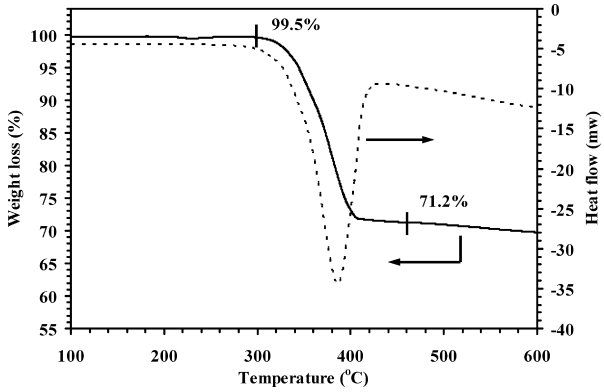

Figure 3. TGA/DSC profile of the $Mg(OH)_2$ product synthesized in hydrothermal treatment with P123 at 240 °C for 72 h without calcination.

one can see that there is a variation in relative signal intensities among the samples due to the difference in crystallinity level. The MgO samples derived hydrothermally with the use of P123 at temperatures ≤ 200 °C (Figure 2b,c) showed XRD signals with intensity weaker than those of their "P123-free" counterparts (Figure 2a). However, when the temperature for hydrothermal treatment was set at 240 °C, the XRD signal intensities of the MgO sample (Figure 2e) derived with P123 were similar to those of the "P123-free" counterpart (Figure 2d). It is common to expect that a nonporous sample would show crystallinity higher than its porous counterparts after high-temperature calcinations. The XRD results displayed in Figure 2 show that, if the temperature for the hydrothermal treatment was raised from 160 to 240 °C, the resulted porous MgO sample shows crystallinity similar to its nonporous counterpart. The results indicated that a higher hydrothermal temperature such as 240 °C is beneficial for the generation of MgO samples of better crystallinity when P123 is employed. It is also observed that the $Mg(OH)_2$ precursor fabricated hydrothermally with P123 at 240 °C for 72 h was single-phase (Figure 2f). Similar results were obtained for the other $Mg(OH)_2$ samples fabricated in the present study.

Figure 3 depicts the representative TGA/DSC profiles of the P123-derived $Mg(OH)_2$ sample collected after hydrothermal treatment at 240 °C for 72 h. There is significant weight loss (28.3%) in the 310−460 °C range accompanied by a well-defined endothermic peak at 389 °C. The weight loss and the endothermic action can be related to the decomposition of $Mg(OH)_2$. The observed weight loss of 29.2% (compared to the *ca.* 28% of other researchers[3c,g,5]) in the 310−550 °C range is only slightly smaller than the theoretical value (30.8%) for complete $Mg(OH)_2$ dehydration. In other words, we had near completion of $Mg(OH)_2$ conversion to MgO at 550 °C.

Representative HRSEM images of the MgO samples fabricated at various treatment temperatures and that of a noncalcined $Mg(OH)_2$ sample are shown in Figure 4. It is observed that the MgO sample acquired after hydrothermal treatment at 160 °C contains mainly hexagonal nanoplates with a thickness of 80−150 nm and a lateral dimension of 0.7−1.2 μm, displaying a morphology totally different from that of the MgO raw material. The morphology and size of these MgO particles are in agreement with those fabricated in hydrothermal processing at 160 °C for 24 h without the addition of a surfactant.[3g] From Figure 4, one can observe that, with a rise in hydrothermal treatment temperature from 160 to 200 °C, there was a formation of rectangular and hexagonal particles. These rectangular and hexagonal particles merged into rectangular parallelepiped and hexagonal prisms, respectively, when the temperature was further increased to 240 °C (Figure 4b−d). The rectangular parallelepiped particles exhibit a lateral length, width, and height of 240−330 nm, 190−250 nm, and 80−120 nm, respectively. As for the hexagonal prism particles, the lateral length and height are 130−210 and 100−460 nm, respectively. One can also see that the morphologies of the $Mg(OH)_2$ particles fabricated hydrothermally with P123 at 240 °C for 72 h were similar to those of the MgO generated after the decomposition of the $Mg(OH)_2$ precursor (Figure 4e,f): 220−550 nm in length, 150−440 nm in width, and 150−240 nm in height for the rectangular parallelepiped $Mg(OH)_2$ particles and 150−900 nm in length and 150−730 nm in height for the hexagonal prism $Mg(OH)_2$ particles. It is clear that the MgO particles have inherited the crystal morphologies of the $Mg(OH)_2$ precursor despite the former having somewhat decreased in dimensions due to shrinkage caused by calcination. The results revealed that the addition of P123 is favorable for the generation of rectangular parallelepiped and hexagonal prisms of $Mg(OH)_2$ and MgO. A similar ability of surfactants in maintaining a hexagonal morphology has been reported before. With ethylenediamine and water in an appropriate ratio, Ding et al. fabricated $Mg(OH)_2$ with a hexagonal lamellar morphology under hydrothermal conditions.[3c] It was pointed out by Li et al. that ethylenediamine played a crucial role in determining the shape of the product particles.[6] Doxsee et al. pointed out that the selective interaction of the coordinating agent with the surface Mg^{2+} ions would slow down the growth rate of specific lattice planes and thus enhance the expression of those planes on the final products.[7] It is generally accepted that the original morphologies of the $Mg(OH)_2$ precursors and the conditions of dehydration processes have important effects on the morphology of the as-generated MgO crystallites. Working on template-induced morphological preservation and self-assembly of MgO nanocrystallites using poly(*N*-vinyl-2-pyrrolidone) (PVP) as an organic template, Ding and Qu[8] observed that the MgO product displayed a hexagonal lamellar-like morphology rather similar to that of the $Mg(OH)_2$ precursor and ascribed such a preservation of particle shape to the presence of the organic template PVP (that transcribed the morphologies of $Mg(OH)_2$ precursors)

(5) (a) Wang, J. A.; Novaro, O.; Bokhimi, X.; López, T.; Gómez, R.; Navarrete, J.; Llanos, M. E.; López-Salinas, E. *Mater. Lett.* **1998**, *35*, 317. (b) Ardizzone, S.; Bianchi, C. L.; Fadoni, M.; Vercelli, B. *Appl. Surf. Sci.* **1997**, *119*, 253.

(6) Li, Y. D.; Liao, H. W.; Ding, Y.; Qian, Y. T.; Yang, L.; Zhou, G. E. *Chem. Mater.* **1998**, *10*, 2301.

(7) Doxsee, K. M.; Chang, R. C.; Chen, E.; Myerson, A. S.; Huang, D. P. *J. Am. Chem. Soc.* **1998**, *120*, 585.

(8) Ding, P.; Qu, B. *Mater. Lett.* **2006**, *60*, 1233.

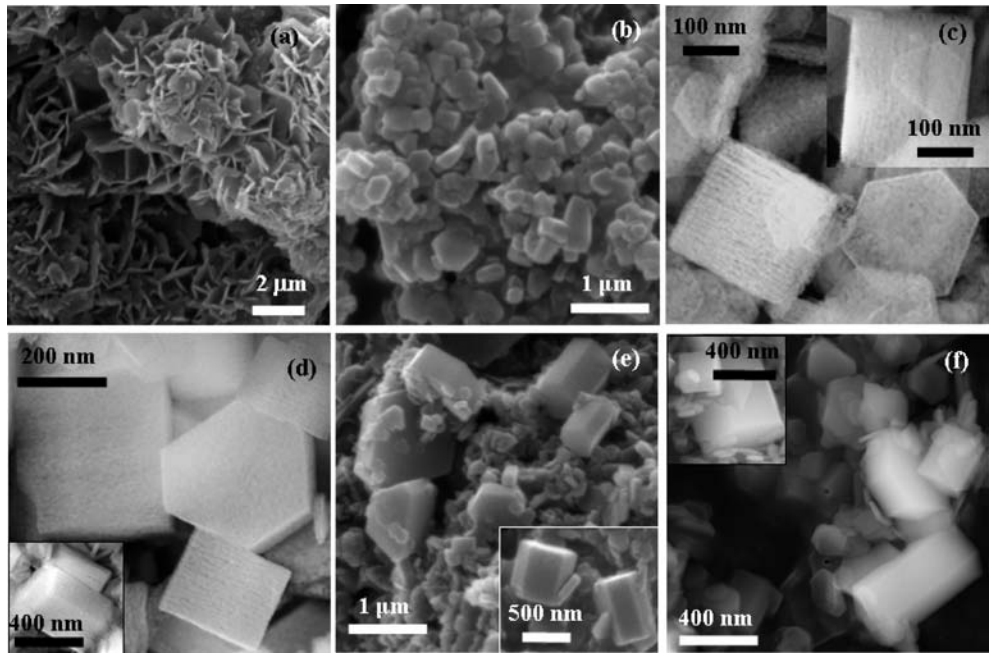

Figure 4. HRSEM images of MgO (a−d) collected after hydrothermal treatment at (a) 160 °C, (b) 200 °C, and (c, d) 240 °C for 72 h and calcination at 550 °C for 3 h and of $Mg(OH)_2$ (e and f) collected after hydrothermal treatment at 240 °C for 72 h without calcination.

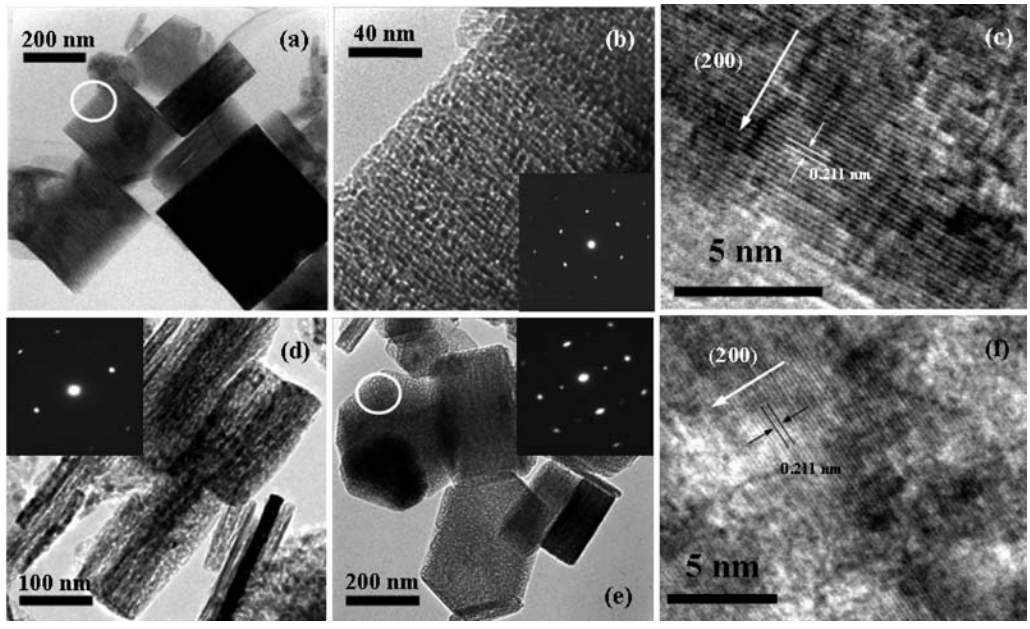

Figure 5. HRTEM images and SAED patterns (insets) of MgO collected after hydrothermal treatment with P123 at 240 °C for 72 h and calcination at 550 °C for 3 h.

and the step-by-step calcination that followed (that governed the nucleation and growth processes). In our present study, the P123 template is expected to have a function similar to that of ethylenediamine or PVP.

The HRTEM and SAED facilities were utilized to determine the morphological and structural features as well as the crystallinity of the MgO materials collected after hydrothermal treatment at 240 °C for 72 h and calcination at 550 °C for 3 h. Shown in Figure 5 are the representative HRTEM images and the corresponding SAED patterns. One can observe the presence of well-defined rectangular parallelepiped (Figure 5a,d,e) and hexagonal prisms (Figure 5e) with roughly ordered 3D wormholelike mesorpores distributed uniformly on the surfaces (Figure 5a,b,d,e). The *d* spacing of the (200) plane was estimated to be 0.211 nm (Figure 5c,f), which is similar to the value of XRD investigation (JCPDS No. 45-946). Furthermore, the highly symmetrically arranged bright spots of the SAED patterns (insets of Figure 5b,d,e) indicated the formation of well-grown single crystallites.

In order to gain insight into the effect of P123 on the morphology of the MgO product, we synthesized a MgO sample hydrothermally without the use of P123, and the HRSEM and HRTEM images of the so-acquired sample are

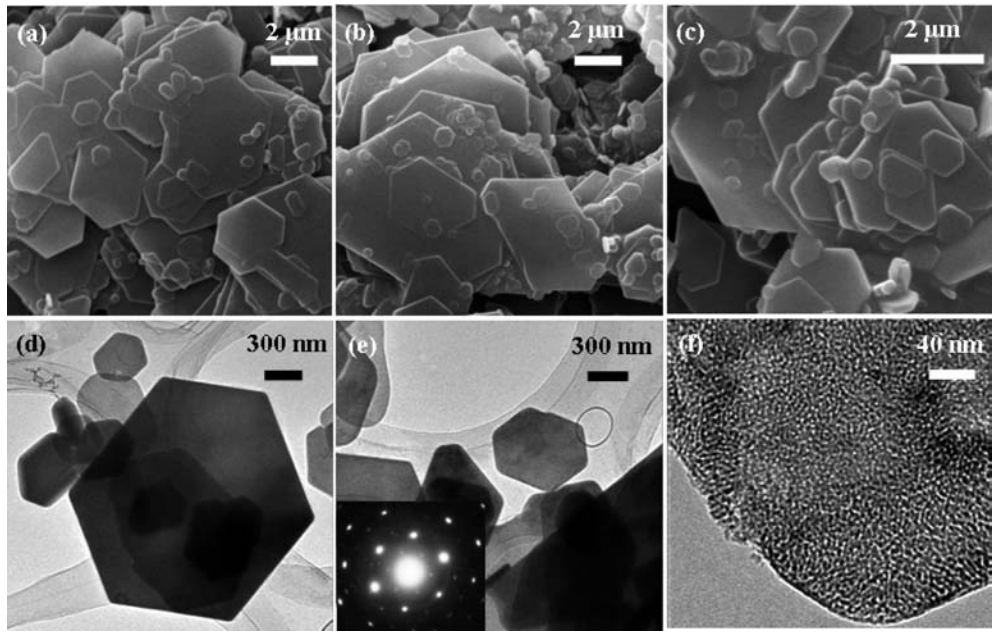

Figure 6. SEM (a−c) and HRTEM (d−f) images as well as the SAED pattern (inset) of MgO collected after hydrothermal treatment in the absence of P123 at 240 °C for 72 h and calcination at 550 °C for 3 h.

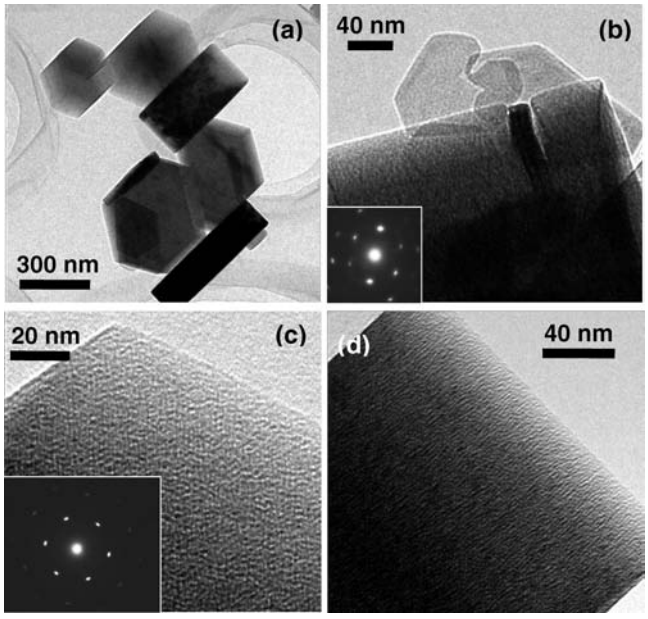

Figure 7. HRTEM images and SAED patterns (insets) of $Mg(OH)_2$ obtained after hydrothermal treatment with P123 at 240 °C for 72 h without calcination.

shown in Figure 6. It is observed that the MgO fabricated without P123 at 240 °C for 72 h and calcined at 550 °C for 3 h exhibits exclusively hexagonal morphology of broad size distribution (lateral length: 200 nm to 6 μm; Figure 6a−c); there is also the presence of wormholelike pores with a diameter and wall thickness of 2−4 nm (Figure 6d−f). The symmetrical pattern of electron diffraction (inset of Figure 6e) confirms the single crystallinity of the MgO sample. The HRTEM images and SAED patterns of the $Mg(OH)_2$ precursor fabricated hydrothermally at 240 °C for 72 h are shown in Figure 7. One can see that the $Mg(OH)_2$ sample contained rectangular parallelepiped and hexagonal entities displaying wormholelike microporous structures (Figure 7c,d). The SAED patterns reveal that the $Mg(OH)_2$ entities are single crystallites.

3.2. Porosity and Surface Area. Figure 8 shows the N_2 sorption isotherms of the MgO samples collected after hydrothermal treatments at different temperatures and calcination at 550 °C for 3 h. The N_2 sorption isotherms of the $Mg(OH)_2$ sample synthesized at 240 °C for 72 h but without calcinations are also shown. The absence of an adsorption isotherm plateau at relative pressure near unity suggested the presence of macropores,[9] whereas the appearance of the hysteresis loop in the p/p_0 range of 0.5−0.9 indicated the presence of mesopores.[10] The N_2 sorption isotherm and pore size distribution of the MgO sample synthesized without P123 under similar conditions are not shown here because they resemble those of the MgO sample reported in the literature.[3g] From Figure 8A(f), one can see that the $Mg(OH)_2$ sample shows a type III isotherm with a H_3 hysteresis loop[11] that can be related to the formation of slit-shaped pores in the aggregates of platelike particles. Apparently, there are macropores as well as micropores (as reflected in the HRTEM investigations) in the $Mg(OH)_2$ sample. In the case of the MgO sample fabricated at 240 °C for 72 h and calcined at 550 °C for 3 h (Figure 8A(e)), besides a H_3 hysteresis loop similar to that of the $Mg(OH)_2$ sample, there is the appearance of a larger hysteresis loop. Such a phenomenon of dual hysteresis loops is common among the three P123-derived MgO samples (Figure 8A(b,c,e)). In other words, there is a presence of mesopores as well as macropores in the P123-derived MgO samples. As shown in Figure 8B(a,d), the small-angle XRD profile of the MgO sample derived

(9) Li, W. C.; Lu, A. H.; Weidenthaler, C.; Schüth, F. *Chem. Mater.* **2004**, *16*, 5676.
(10) Gou, L.; Murphy, C. J. *J. Mater. Chem.* **2004**, *14*, 735.
(11) Gregg, S. J.; Sing, K. S. W. *Adsorption, Surface Area and Porosity*, 2nd ed.; Academic Press: London, UK, 1982.

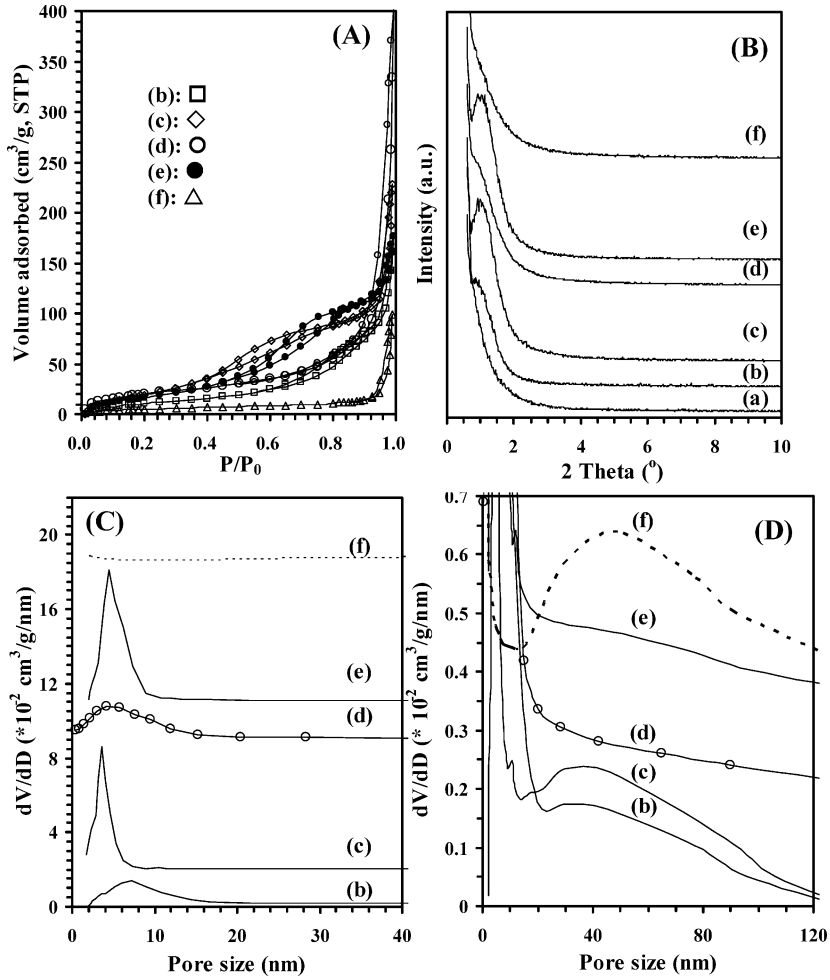

Figure 8. (A) Nitrogen adsorption−desorption isotherms, (B) small-angle XRD patterns, and (C, D) pore size distributions of MgO samples generated hydrothermally and calcined at 550 °C for 3 h (a) without P123 at 160 °C for 24 h, (b) with P123 at 160 °C for 72 h, (c) with P123 at 200 °C for 72 h, (d) without P123 at 240 °C for 72 h, and (e) with P123 at 240 °C for 72 h and (f) that of $Mg(OH)_2$ collected after hydrothermal treatment with P123 at 240 °C for 72 h without calcination.

Table 1. Synthetic Conditions and Texture Parameters of MgO and $Mg(OH)_2$

				BET surface area (m^2/g)		pore volume (cm^3/g)		
sample	surfactant	hydrothermal conditions (°C and h)	calcination conditions (°C and h)	macropore (>38 nm)	mesopore (<38 nm)	macropore (>38 nm)	mesopore (<38 nm)	average pore size (nm)
MgO		160 and 24	550 and 3	3	101	0.02	0.23	11.1
MgO		160 and 72	550 and 3	4	100	0.03	0.23	11.0
MgO	P123	160 and 72	550 and 3	2	104	0.04	0.24	17.7
MgO	P123	200 and 72	550 and 3	10	133	0.17	0.22	8.0
MgO		240 and 72	550 and 3	5	103	0.02	0.24	15.8
MgO	P123	240 and 72	550 and 3	1	297	0.03	0.42	7.6
$Mg(OH)_2$	P123	240 and 72		7	13	0.04	0.11	29.3

without P123 at 160 °C for 2 h followed by calcination at 550 °C for 3 h showed no detection of diffraction peaks, but that of the MgO sample derived without P123 at 240 °C for 2 h followed by calcination at 550 °C for 3 h showed a weak diffraction signal at $2\theta = ca.\ 1°$. The results indicated that a rise in temperature for hydrothermal treatment results in improvement in uniformity of the pore structure. As for the MgO samples derived with the assistance of P123, the intensity of the peak at $2\theta = ca.\ 1°$ is relatively more intense (Figure 8B(b,c,e)), demonstrating that the introduction of P123 is beneficial for the formation of mesopores in MgO. The $Mg(OH)_2$ sample showed no signal of small-angle diffraction (Figure 8B(f)), confirming the absence of mesopores in the $Mg(OH)_2$ precursor as revealed in HRTEM investigation.

The texture parameters of the as-synthesized MgO and $Mg(OH)_2$ samples are summarized in Table 1. As evidenced by the pore size distributions of the samples (Figure 8C), the MgO sample synthesized hydrothermally without P123 at 240 °C for 72 h and calcined at 550 °C for 3 h showed a broad distribution of pore size (Figure 8C(d)). The pore size distribution of the MgO sample derived with P123 at 160 °C for 72 h and calcined at 550 °C for 3 h is also wide in pore size distribution (Figure 8C(b)), and the average pore diameter is *ca.* 17.7 nm. Raising the treatment temperature to 200 or 240 °C would give rise to a narrower pore size

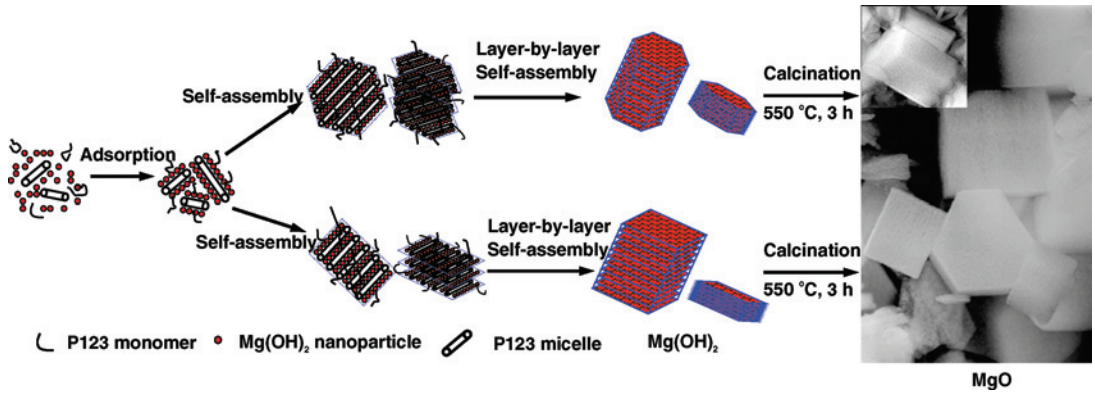

Figure 9. Schematic illustration of the formation of rectangular parallelepiped and hexagonal prism $Mg(OH)_2$ and the corresponding mesoporous MgO.

distribution (Figure 8C(c,e)) with an average pore diameter of *ca.* 8.0 and 7.6 nm, respectively (Table 1). As for the $Mg(OH)_2$ sample, the pore size distribution is very wide, and the average pore diameter of *ca.* 29.3 nm (Table 1) suggests the presence of micropores and macropores as disclosed in the HRTEM observations (Figure 7c,d) as well as in the enlarged profile of pore size distribution in the ranges of 0−10 nm and 10−120 nm (Figure 8D(f)). It should be noted that all of the samples possess macropores (Figure 8D). We find that, despite the surface areas of the MgO samples fabricated hydrothermally with or without P123 at 160 °C for 24 or 72 h and without P123 at 240 °C for 72 h being similar to that (97 m^2/g) of the sample reported by Yu et al.,[3g] the MgO samples synthesized by us with P123 at 200 and 240 °C followed by calcination at 550 °C for 3 h possess much larger surface areas (143 and 298 m^2/g, respectively) and pore volumes (0.39 and 0.45 cm^3/g, respectively). The surface area of the MgO sample fabricated with P123 at 240 °C is much higher than that (*ca.* 150 m^2/g) of the MgO sample derived using a carbon aerogel template,[9] and close to that (306 m^2/g) of ordered mesoporous MgO derived using a CMK-3 exotemplate.[3e] The much lower surface area of the $Mg(OH)_2$ sample obtained in hydrothermal treatment with P123 at 240 °C further confirms the presence of micropores and macropores. With $Mg(OH)_2$ being dehydrated during calcination, mesopores are generated due to the shrinkage of macropores, resulting in significant enhancement of the surface area and pore volume. It can also be observed from Table 1 that the contribution of the macropores to the BET surface areas and pore volumes of the as-synthesized MgO samples is rather small, with the P123-derived MgO sample fabricated at 200 °C for 72 h (calcined similarly at 550 °C for 3 h) being the only exception. One can see that there are relatively more macropores in the sample fabricated at 200 °C, and the macropores contribute to *ca.* 7 and 44% of the total BET surface area and pore volume, respectively. That is to say, after calcination at 550 °C for 3 h, the MgO sample derived hydrothermally with P123 at 200 °C for 72 h possesses a larger amount of macropores, which are likely to be present inside the MgO entities as well as between the MgO particles.

3.3. Formation Mechanism. It is known that, with a rise in temperature of the triblock P123 copolymer (PEO−PPO−PEO), there is an increase in hydrophobicity of the PPO moiety and decrease in hydrophilicity of the PEO moiety, and the cloud point of P123 in a 1 wt % aqueous solution is around 90 °C.[12] Under the high-temperature (200−240 °C) hydrothermal conditions adopted in the present study, the micellization and phase transformation behaviors of P123 are different from those under the low-temperature (80−160 °C) conditions. Figure 9 illustrates the possible formation mechanism of the rectangular parallelepiped and hexagonal prism $Mg(OH)_2$ and porous MgO. Under hydrothermal conditions, bulk MgO powders hydrolyze into primary $Mg(OH)_2$ nanoparticles that arrange in quadrangle or hexagonal arrays with the P123 micelles adsorbed preferably on the well-aligned $Mg(OH)_2$ surfaces either through hydrogen bonding with the OH groups connected to Mg^{2+} or through loose coordination with Mg^{2+}.[10] Such a kind of selective adsorption has been reported by Wang et al.,[13] who believed that the preferential adsorption of nonionic polyethylene glycol (PEG 4000) on the $Mg(OH)_2$ crystal planes facilitated the formation of platelike MgO nanostructures. The interaction of the surfactant and magnesium has also been reported by Takenaka et al., who evidenced experimentally the formation of $CH_3(CH_2)_nCOOH$−Mg complexes in the form of a lamellar mesophase when $CH_3(CH_2)_nCOOH$ ($n = 10-20$) was used as the surfactant.[14] In the case of using P123 as a surfactant, the extent of P123 adsorption on a $Mg(OH)_2$ plane depends on the surface density of the magnesium atoms.[15] Since the surface density of Mg on the (001) plane is higher than that on the other planes of the $Mg(OH)_2$ crystal,[16] the (001) plane would be blocked preferentially by the adsorbed P123 molecules during the growing process of $Mg(OH)_2$ nanoentities. In other words, growth on the (001) plane would be markedly restricted, and the consequence is the generation of 2D nanoplate-like $Mg(OH)_2$ entities. Other experimental evidence for the selective adsorption of surfactant molecules

(12) BASF Technical Bulletin. http://www.basf.com/businesses/chemicals/performance/pdfs/Pluronic_P123.pdf (accessed Apr 2008).
(13) Wang, W.; Qiao, X. L.; Chen, J. G.; Li, H. J. *Mater. Lett.* **2007**, *61*, 3218.
(14) Takenaka, S.; Sato, S.; Takahashi, R.; Sodesawa, T. *Phys. Chem. Chem. Phys.* **2003**, *5*, 4968.
(15) Zhang, Z.; Sun, H.; Shao, X.; Li, D.; Yu, H.; Han, M. *Adv. Mater.* **2005**, *17*, 42.
(16) Melgunov, M. S.; Fenelonov, V. B.; Melgunova, E. A.; Bedilo, A. F.; Klabunde, K. J. *J. Phys. Chem. B* **2003**, *107*, 2427.

on metal ions comes from Bai et al.[17] and Takenaka et al.[14] With the presence of $Mg(OH)_2$ nanoparticles becoming significant, the quadrangle- or hexagonal-packed $Mg(OH)_2$ entities self-assemble in a layer-by-layer manner[17] into nano- or microsized rectangular parallelepiped and hexagonal prisms. Under high-temperature hydrothermal conditions, surfactants such as P123 might split into fragments, resulting in (i) a high dispersion of most of the fragments in the interstitials and on the surfaces of the arrayed $Mg(OH)_2$ particles via the aforementioned weak interactions or (ii) possible encapsulation of part of the fragments in the $Mg(OH)_2$ aggregates. After removal of the surfactant in large quantity by means of washing with deionized water and ethanol, and with the subsequent calcination at 550 °C, the rectangular parallelepiped and hexagonal $Mg(OH)_2$ prisms change into nano- or microscale particles of 3D wormholelike mesoporous MgO single crystallites with a satisfactory preservation of surface morphologies of the $Mg(OH)_2$ precursors. The decomposition of surfactants such as graft copolymers in alkaline solution under high-temperature hydrothermal conditions has also been reported by other researchers.[18]

(17) Bai, P.; Su, F.; Wu, P.; Wang, L.; Lee, F. Y.; Lv, L.; Yan, Z.-F.; Zhao, X. S. *Langmuir* **2007**, *23*, 4599.

(18) (a) Ellis, A. V.; Wilson, M. A. *J. Org. Chem.* **2002**, *67*, 8469. (b) Sun, C.; Sun, J.; Xiao, G.; Zhang, H.; Qiu, X.; Li, H.; Chen, L. *J. Phys. Chem. B* **2006**, *110*, 13445. (c) Yang, B. Y.; Montgomery, R. *J. Carbohydr. Res.* **1996**, *280*, 27. (d) Luijkx, G. C. A.; van Rantwijk, F.; van Bekkum, H.; Antal, M. *J. Carbohydr. Res.* **1995**, *272*, 191.

4. Conclusions

In summary, 3D wormholelike mesoporous single-crystalline nano- and microsized MgO displaying morphologies of rectangular parallelepiped and hexagonal prisms have been fabricated using the P123-assisted hydrothermal dissolution−recrystallization method. The mesoporous MgO product with the highest surface area (298 m^2/g) was fabricated after hydrothermal treatment at 240 °C for 72 h followed by calcination at 550 °C for 3 h. It is suggested that the introduction of surfactants (P123) and the increase of hydrothermal treatment temperature favor the generation of rectangular parallelepiped and hexagonal prism MgO single crystallites of high surface area.

Acknowledgment. This work was financially supported by the NSF of China (Grant No. 20473006), the SRF for ROCS (State Education Ministry of China), the PHR (IHLB) of Beijing Municipality, and the HKBU (Grant No. FRG/06-07/II-10).

IC7015462